IMAGE BASED SAR PRODUCT SIMULATION FOR ANALYSIS

G. Domik and F. Leberl
VEXCEL Corporation
Boulder, Colorado 80301

ABSTRACT

SAR product simulation serves to predict SAR image grey values for various flight paths. Input typically consists of a digital elevation model and backscatter curves. We describe a new method of product simulation that employs also a real SAR input image for image simulation. This can be denoted as "image-based simulation". Different methods to perform this SAR prediction are presented and advantages and disadvantages discussed. Ascending and descending orbit images from NASA's SIR-B experiment were used for verification of the concept: input images from ascending orbits were converted into images from a descending orbit; the results are compared to the available real imagery to verify that the prediction technique produces meaningful image data.

1. INTRODUCTION

Computer based SAR image simulation has always been of great interest, because it permits one to test SAR processing components and to bypass costly SAR data collection for parameter studies. The type of simulations in use, their variety of input parameters, their intermediary and final results differ widely due to a wide spread of applications. A complete SAR simulation process must include the simulation of a radar transmitter, receiver, the operation of a signal processor and the output of a radar image. Most of the currently existing simulators, however, treat only a particular aspect of the whole process, addressing a specific problem and application. An all-purpose SAR-simulator would need to deal with a very complicated process and would require considerable expense in both development as well as application.

A report by Marconi Research Center (1984), reviewed existing SAR simulators and divided them into two groups, specifically "system" and "product" simulators. System simulators model the complete SAR process whereas product simulators model only the necessary steps to produce a synthetic image with as much likeness to a corresponding real radar image as desired. An example for a system simulator is SARSIM (D. Farquharson et al., 1977), developed by Ferranti Ltd. and implemented at the European Space Research and Technology Centre (ESTEC) in Nordwijk, The Netherlands; well known product simulators are the Kansas Simulator (J.C. Holtzman et al., 1978), its upgraded versions at the University of Berlin and the DFVLR (Sieber et al., 1985), and the simulator at the University of Arkansas (Kaupp, 1982).

In a series of small research efforts ongoing since 1982 two product simulators were developed by Domik (e.g. 1985). The simulators were modeling a component of the SAR process, namely geometric positioning, by relating terrain locations to image pixels. The simulators served to analyze radar images, provided an intermediary step for a digital rectification procedure and supplied necessary data sets for stereo investigation studies which were not available with real data. Because only limited attempts were made in the simulation to model backscatter from different targets, speckle and resolution, the image product lacked visual realism. Whereas this did not administer any problems in the case of rectification or image analysis methods, it limited the utility in stereo studies because the effect of speckle and micro-detail on stereo visibility could not be investigated.

An interesting alternative to image simulation based on terrain data is one based on imagery itself. In this case an input image is transformed into an output image. The concept was employed in the SIDEVIEW project for optical imagery (ESL, 1985).

The current paper presents a novel method for SAR product simulation that transforms a given SAR image into one as if it were taken from an entirely different flight path and with a different sensor geometry. The result can be useful for classical applications of simulation such as training, for parameter studies and as a tool for SAR image interpretation.

2. INPUT DATA DESCRIPTION

Various SAR prediction methods are described in the following chapter. Actual input data for numerical work was based on SIR-B SAR and topographic data, namely:

(a) SIR-B image (ascending orbit, Data Take 92.8) with a center incidence angle of 31.4°. Flight path (South-West to North-East) was 48° from North. Illumination direction to left.

(b) SIR-B image (descending orbit, Data Take 56.4) with a center incidence angle of 32.9°. Flight path (North-West to South-East) was 128° from North. Illumination direction to left.

(c) Flight path and imaging parameters for both data takes as provided on the header of the magnetic tape with the digital images.

(d) Digital elevation model (DEM) created from aerial photography. Accuracy is expected to be about $\pm$7m. The elevation data collected were in the form of contour lines and were converted to a grid with a 37.5m spacing. It needs to be understood that a DEM represents only the "macro-relief"; the relevant micro-relief is presented in a SAR image but will typically not be shown in the DEM.

Both SIR-B images (Figures 1 and 3) had originally a pixel size of 12.5 m and were resampled to 37.5m/pixel. Image (a) is used as an input to the prediction methods, (b) is used for comparison with resulting synthetic images.

A landmark feature for visual comparison of the images is the town of "Jose de San Martin" in the lower (sourthern) part of the pictures. Because the illumination direction happens to be perpendicular to the major street direction of the town in the descending path, extremely bright specular radar returns do result. The different flight path of the ascending image does not show such specular returns.

The digital elevation model does not need to be taken from aerial photography. The data could also have been extracted from stereo radar images or from an existing map.

3. PREDICTION (SIMULATION) TECHNIQUES

The input consists of the digital elevation model and one real radar image representing the area of interest. Additionally one needs flight and imaging parameters to model the radar sensor situation both for the original radar image and the image to be predicted.

First, a digital radar ortho image is created using a multi-step radar image rectification method described by Domik et al., (1986). Additionally, some of the prediction methods also require a radiometrically rectified image; this is defined as a radar ortho image with the effect of topographic slope on image brightnesses removed or reduced. In the present case the radar ortho image (and its slope-reduced version) is derived from one ascending SIR-B path. The descending image is predicted.

Figures 1 to 6 present the input, intermediate image products and the final result. Fig. 1 displays the radar ortho image of the ascending path, Fig. 2 the corresponding radiometrically rectified (slope-reduced) image. Figure 3 presents the original radar ortho image from the descending path for comparison with the results from prediction methods A, B, and C in Figures 4, 5 and 6, respectively.

The following describes the three prediction methods and their underlying physical justification.

3.1 Method A: Varying Muhleman's Constant

Muhleman's (1964) backscatter curve establishes a relationship between radar backscatter of rough surfaces and corresponding incidence angles on the ground:

$$\text{(Eq. 1)} \qquad \sigma_m = \log_{10} \frac{A^3 * \cos \theta^i}{(\sin \theta^i + A^* \cos \theta^i)^3}$$

We assume in this prediction method that the imaged terrain consists of a number of scatterers which can be modeled by

Eq. 1, the difference being variable "A" (the Muhleman's constant). We can compute A from each input pixel gray value (DN number), i.e. for each pixel of the ascending image:

$$(Eq.2) \qquad A = \frac{\sin \theta^i}{\sqrt[3]{\frac{\cos \theta^i}{10\sigma}} - \cos \theta^i}$$

The input incidence angle θ^i is obtained from the DEM to which the image was registered.

A new incidence angle is calculated for each DEM cell from flight and imaging information of the output image from the descending path and the slope/height information of the terrain. By employing Eq. 1 using the computed "A" and the new incidence angle, a new σ_m and image gray or DN value is assigned to each pixel. This is the predicted backscatter for a radar image from descending orbit.

Work steps: (σ .. sigma; θ^i .. inc. angle)

$\sigma_{asc.}$ combined with $\theta^i_{asc.}$ $\xrightarrow{\text{Eq. 2}}$ Muhleman's A; combined with $\theta^i_{desc.}$ $\xrightarrow{\text{Eq. 1}}$ $\sigma_{desc.}$

The resulting image is presented in Figure 4. One might argue against that technique with the observation that the brightness change from one pixel to the next might be due to changes in slope, as the available DEM does not reflect the micro relief. Prediction method A will always interpret the grey values as a function of the incidence angle (in the macro relief given by the input DEM) and a thematic factor (the Muhleman's constant). Also, features with backscatter properties different from a diffuse scatterer (e.g. towns, rivers and roads) cannot be predicted from the input image.

3.2 Method B: Using a Local SIR-B Backscatte Distribution Curve

In this case we assume that the radiometrically rectified image is indeed void of effects of relief. What is seen in the resulting image under this assumption is a thematic effect independent from illumination direction and terrain slope (Figure 2).

The radar ortho image and corresponding incidence angles from the ascending input image serve to quantify the back-scatter properties of the macro relief by plotting the average values of backscatter vs. incidence angles. This backscatter curve (or lookup table) replaces the previously used Muhleman's curve and is referred to as the "local SIR-B backscatter curve".

In a first step a synthetic image is created using the DEM and the local SIR-B backscatter curve. This synthetic image is merely an illuminated relief model and does not display any speckle effect. Subsequently the radiometrically rectified image is multiplicatively superimposed on the illumination, resulting in Figure 5.

Method B has the same shortcomings as the previous method. It is for example obvious that specular reflections cannot be predicted from the input image.

3.3 Method C: Deriving Micro Relief from Grey Values

Again we assume that the backscatter distribution in the SIR-B image follows the Muhleman's backscatter curve (Eq. 1) with a constant A = 0.2 (terrain is a homogenous, diffuse scatterer in the area imaged). The grey value distribution is assumed to be entirely dependent on the occurring incidence angles, which in turn are a combination of terrain slope and elevation angle. Because of the nature of radar and its geometric resolution of 14 m in the case of SIR-B, the grey values reflect backscatter from micro relief not visible in the height model. To compute the incidence angle corresponding to a certain grey value one conveniently creates first a lookup table (inverse Muhleman's lookup table denoted by f^{-1}) relating grey values to incidence angles; then one assigns an incidence angle to each occurring image grey value in the ascending image. From the incidence angle one unambiguously derives the slope in range direction if one neglects the slope in azimuth direction. Processing the input image pixel by pixel via the above described method, a file with new slopes in the range direction is created, describing the hypothetical micro relief of this area.

When predicting SAR brightness values for a new sensor situation (e.g. a descending path) the new slopes are used together with flight and imaging parameters to define new incidence angles. Eq. 1 then assigns a grey value to each incidence value (A is still kept constant at 0.2). This grey value then represents the predicted value for a SAR at the defined descending path (Fig. 6).

Work steps: (σ .. sigma; Θ^i .. inc. angle; Θ .. elev. angle)

$$\sigma_{asc.} \xrightarrow{f^{-1}} \Theta^i_{asc.} \longrightarrow \text{slope; combined with}$$

$$\Theta_{desc.} \longrightarrow \Theta^i_{desc.} \xrightarrow{\text{Eq. 1}} \sigma_{desc.}$$

Error sources in this case will be areas where the grey values display a great dependency on their thematic properties, e.g. towns, different geological units, etc. The concept of determining micro-relief must not neglect slopes in azimuth direction. The current implementation does neglect these slopes and will need to be improved using what Wildey (1986) calls radar clinometry.

4. DISCUSSION OF RESULTS

Visual comparison shows that the best correspondence between predicted and original can be observed in the result of method B. This is mainly an effect of using the local rather than Muhleman's backscatter curve. Method C has the temporary shortcoming of using Muhleman's curve in the course of the algorithm instead of the local SIR-B backscatter curve. Obviously none of the algorithms can model specular returns and correctly change the backscatter when imaging the town of Jose de San Martin. The information necessary to model this type of reflection is beyond the currently acceptable level of cost and complexities.

If the modeling of radar echoes needs to account for specular and in homogeneous targets more sophisticated approaches e.g. Sieber et al. (1985) must be introduced, and sufficient input data must be available. (e.g. in the form of backscatter data bases) description of man made features. The methods presented here serve to assist in some aspects of training in the use of and analysis of SAR images. They represent comparatively fast and efficient product simulation tools. Their main advantage is the absence of a need for elaborate databases. Only the macro relief is required in the form of a DEM; planimetric data with SAR-relevant attributes are avoided.

ACKNOWLEDGEMENT

This effort represents results of one phase of research performed under JPL contract No. 957549, subtask "Jose de San Martin". The contract is managed by Dr. JoBea Cimino. We are grateful for her encouragement.

REFERENCES

Domik G., 1985:
"Verfahrensentwicklungen zur Analyse von digitalen Seitsicht-Radarbildern gebirgigen Gelaendes mittles digitaler Hoehenmodelle und Bildsimulation". Doctoral Thesis. Technical University Graz, Austria. 173 pages.

Domik G., F. W. Leberl and J. B. Cimino, 1986:
"Multiple Incidence Angle SIR-B Experiment Over Argentina: Generation of Secondary Image Products". IEEE Transactions on Geoscience and Remote Sensing, July 1986, Volume GE-24, No. 4. Special issue on the Shuttle Imaging Radar (SIR-B). pp. 492-497.

ESL, 1985:
"Image Transformation Study". Techn. report Rep. # ER443, 4 Feb 1985. ESL, Sunnyvale, CA 94086.

Farquharson D. et al., 1977:
"Description of a Simulation Model of Synthetic Aperture Radar Systems", Ferranti Ltd., Final Report (4 volumes), Report Number 2831, July 1977.

Holtzman J.C., V.S. Frost, J.L. Abbott, V.H. Kaupp, 1978:
"Radar Image Simulation". IEEE Trans. Geosci. Electron. GE-16, 4, October 1978.

Kaupp V.H., L.C. Brigdes, M.A. Pisaruck, H.C. MacDonald, W.P. Waite, 1982:
"Comparison of Simulated Stereo Radar Imagery". International Geoscience and Remote Sensing Symposium, June 1-4, 1982; Munich. pp. TA-4, 2.1-2.5.

Marconi Research Centre, 1984:
"SAR Simulation Concept and Tools". Final report prepared for the ESA under Contract No. 5430/83/GP-I by the Remote Sensing Group, MSDS Reserach Lab., Marconi Research Centre, Chelmsford, Essex. 109 pages.

Muhleman, 1964:
"Radar Scattering from Venus and the Moon". Astronomical Journal, Vol. 69, p. 34.

Sieber A., A. Popella, Ph. Hartl, G. Domik, 1985:
"SAR Product Simulation". Final Report prepared for the ESA under ESTEC contract No. 6188/85 NL/BI by the Institute for Navigation, Univ. of Stuttgart, Keplerstr. 11, D-7000 Stuttgart 1. 235 pages.

Wildey R.L, 1986:

"Radarclinometry for the Venus Radar Mapper". Photogr. Engin. and RS, Vol. 52, No.1, Jan. 1986, pp.41-50.

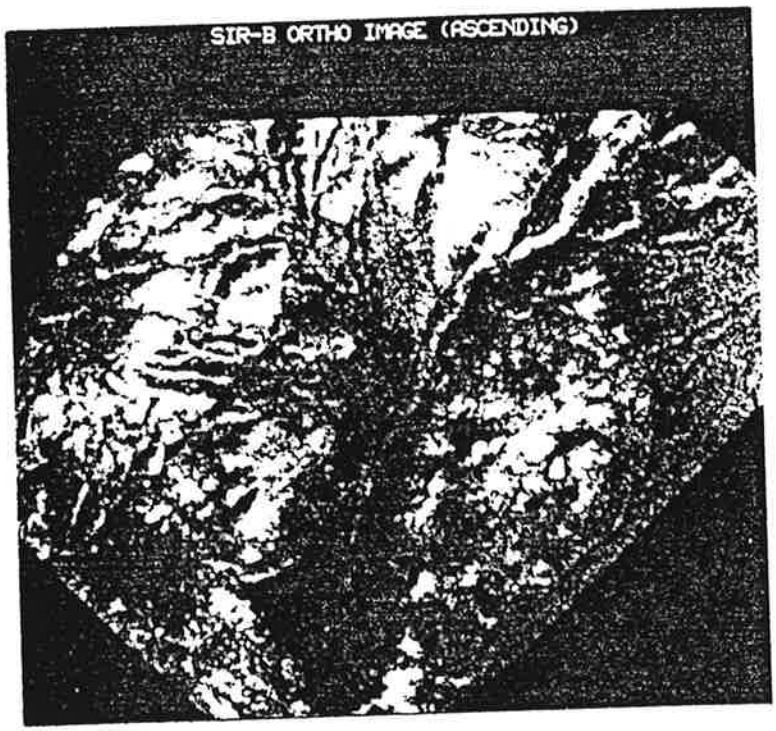

Figure 1: SIR-B D.T. 92.8. Ortho image. North is straight up. Image represents app. 15 x 15 km^2.

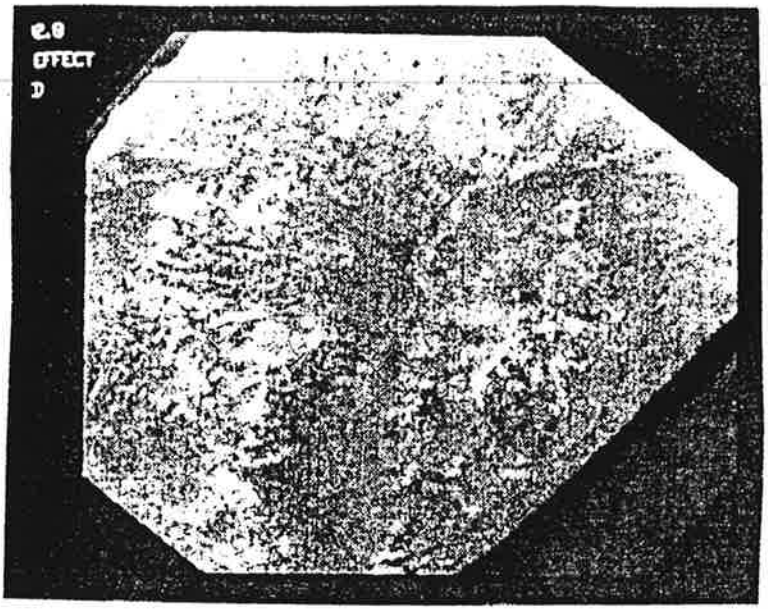

Figure 2: SIR-B D.T. 92.8. Slope-reduced Radar Ortho Image.

Figure 3: SIR-B D.T. 56.4. Ortho Image. North is straight up.

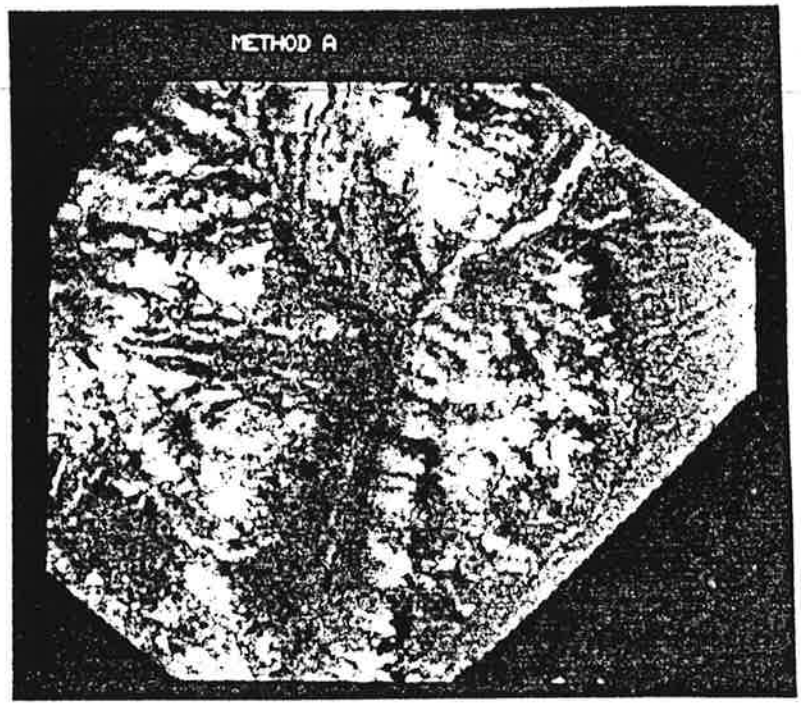

Figure 4: Predicted Radar Image according to "Method A".

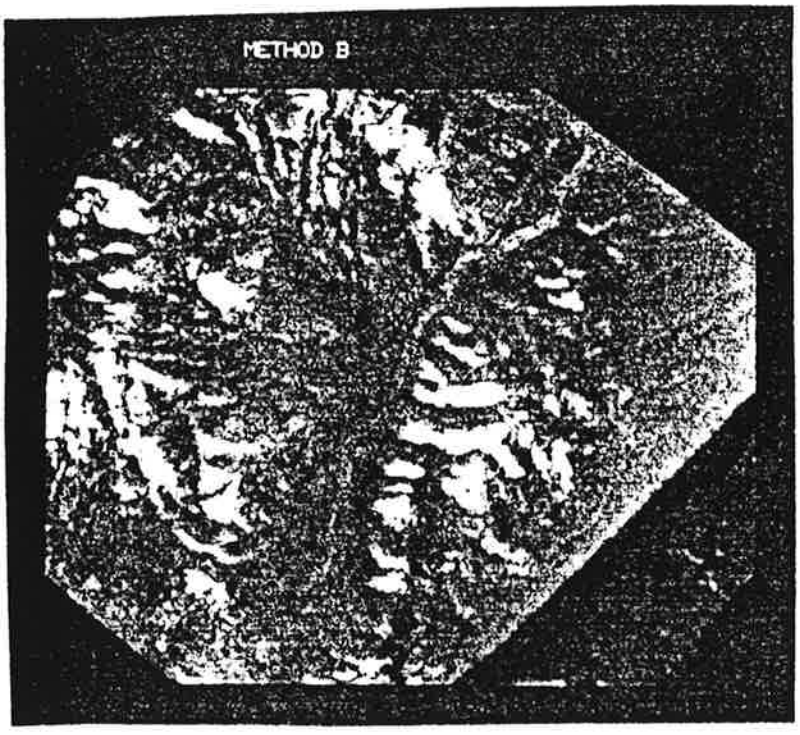

Figure 5: Predicted Radar Image according to "Method B".

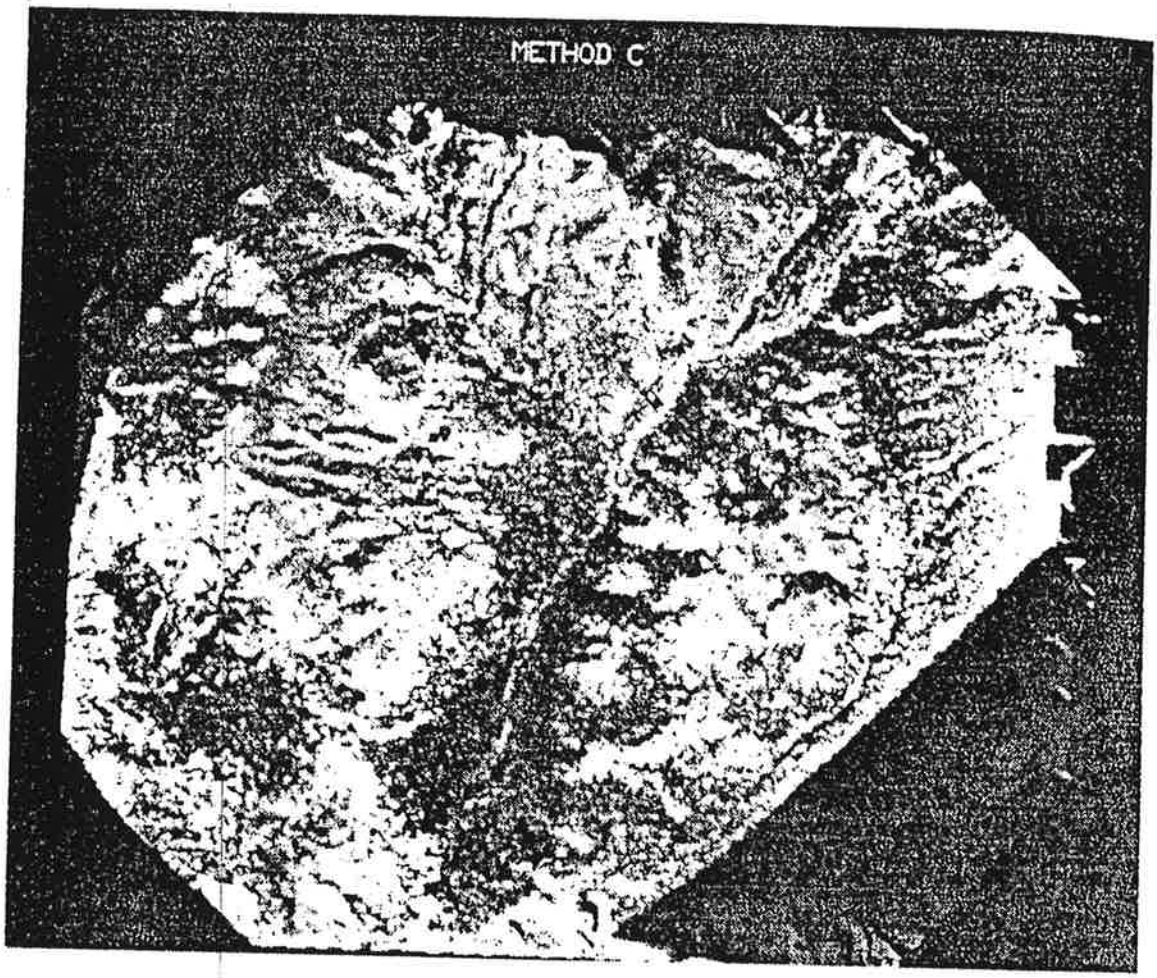

Figure 6: Predicted Radar Image according to "Method C".